Supporting Information

Formation of an Unusual Glutamine Tautomer in a Blue-Light Using Flavin Photocycle Characterizes the Light-Adapted State

Joshua J. Goings, Pengfei Li, Qiwen Zhu, and Sharon Hammes-Schiffer*

Department of Chemistry, Yale University, 225 Prospect Street, New Haven, Connecticut 06520

*Corresponding author email: sharon.hammes-schiffer@yale.edu

www.pnas.org/cgi/doi/10.1073/pnas.2016719117

Table of Contents

A. Computational Details S3

A.1 Simulating reverse proton-coupled electron transfer (PCET) S3

A.2 Protein preparation and equilibration for classical MD S6

A.3 QM/MM calculations of the flavin absorption spectrum and C4=O carbonyl stretch frequency S8

B. Additional computed flavin absorption spectra S11

B.1 Gas phase flavin absorption spectra using ensemble from main text with TDDFT S11

B.2 Flavin absorption spectra using ensemble from main text with TDA-TDDFT S12

B.3 Flavin absorption spectra using additional independent 5 ns ensemble with TDA-TDDFT S13

C. Parameterization of the force field for the glutamine imidic acid tautomer S14

C.1 QM optimized geometry of the model compound S16

C.2 Atom types and partial charges for the Gln imidic acid tautomer S16

C.3 Additional parameters for the CHARMM36 force field for the Gln imidic acid tautomer S16

References S20

A. Computational Details

A.1 Simulating reverse proton-coupled electron transfer (PCET)

To simulate the reverse proton-coupled electron transfer (PCET) process in the Slr1694 BLUF photoreceptor, we started with nine initial conditions (i.e., the solvent and protein coordinates with corresponding velocities) from our previous work.(1) The nine initial conditions correspond to the endpoints of mixed quantum mechanical/molecular mechanical (QM/MM) molecular dynamics (MD) trajectories that showed the forward PCET process after photoexcitation of the flavin. Specifically, these trajectories showed electron transfer from Tyr8 to the flavin, followed by double proton transfer from Tyr8 to the flavin using excited state TDA-TDDFT calculations followed by ground state spin-flip TDA-TDDFT calculations at the LRC-ωPBEh/6-31G* level of theory.(2-6) The details for the preparation of these initial conditions can be found in Ref (1). Briefly, this initial system corresponds to a solvated diradical Slr1694 BLUF domain obtained from PDB 2HFN chain D, where the FMN is in the $FMNH^{\bullet}$ radical state, Tyr8 is in the unprotonated neutral tyrosyl radical state, $Tyr\text{-}O^{\bullet}$, and Gln50 is in the rotated imidic acid tautomer form.

The current QM/MM molecular dynamics (MD) simulations were performed using the same protocol as the previous simulations. The QM region consisted of FMN, Gln50, and Tyr8. Hydrogen link atoms were placed between the C_α and C_β atoms of Tyr8, the C_β and C_γ atoms of Gln50, and the C1′ and C2′ atoms of FMN. A diagram of the QM region including link atoms is given in Fig. S1. The charge on the MM host atom was set to zero and redistributed over the rest of the atoms in the group. Each QM host C–H bond had an equilibrium length of 1.111 Å. Including the link atoms, the QM region consisted of 56 atoms. All QM/MM calculations were

performed using the CHARMM/Q-Chem interface.(7-9) The protein was solvated in a spherical water shell with a 36 Å radius centered at the Gln50 C_α, with all solvent molecules beyond a 28 Å radius centered at the Gln50 C_α frozen. The overall system was charge neutral, with Na^+ and Cl^- ions providing the compensating charges, and additional ions were included to produce a NaCl concentration of approximately 0.150 M. All bonds involving hydrogen atoms were constrained using the SHAKE algorithm.(10) A 1 fs time step was used for all QM/MM MD simulations.

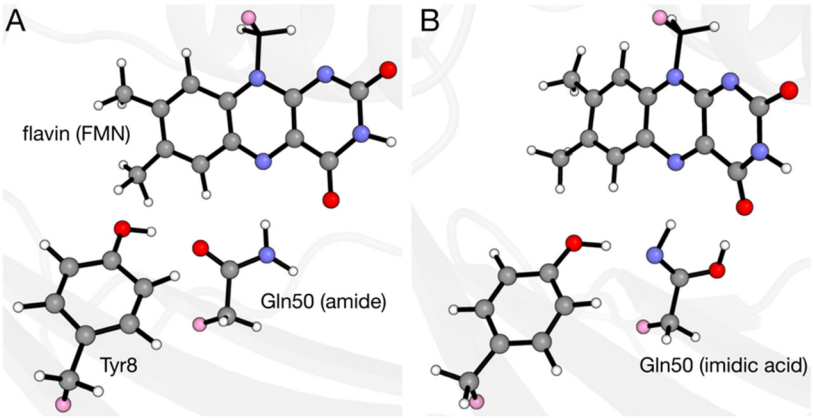

Fig. S1. Schematic of the QM region used in this study, consisting of the flavin (FMN), tyrosine, and glutamine for (A) the amide form of the glutamine (dark-adapted state) and (B) the imidic acid form of the glutamine (light-adapted state). Link atoms are shown as pink spheres. Both QM regions have the same number and type of atoms.

Given these initial conditions, to simulate the reverse PCET process, we enforced charge recombination by constraining the system to be in the closed-shell ground state at the LRC-ωPBEh/6-31G* level of theory. In other words, we switched to conventional closed-shell DFT instead of spin-flip TDA-TDDFT. This procedure corresponds to instantaneously repairing the electrons, which transfers an electron from the protonated flavin radical to the unprotonated tyrosine radical, i.e., $FMNH^\bullet$ becomes $FMNH^+$ and Tyr-$O^\bullet$ becomes Tyr-O^-. This charge recombination leads to a charge-separated state in the active site. Of the nine trajectories simulated, four of the trajectories showed the protons rapidly transfer (all within 250 fs) from the flavin back

to the tyrosine via a double proton transfer mechanism, as discussed in the main text, to form the light-adapted state characterized by the rotated Gln50 imidic acid tautomer.

Of the nine trajectories used to simulate the reverse PCET reaction, five of the trajectories did not show the formation of the light-adapted state. Three of the unproductive trajectories followed a reverse PCET mechanism that moved the protons back to the original dark-adapted state (i.e., reformed the amide tautomer of the Gln50 residue), as shown in Fig. S2A and S2B. For two trajectories, the charge recombination procedure led to the formation of an unphysical Tyr8-Gln50 adduct (Fig. S2C-F). These unphysical adducts are probably an artifact of suddenly constraining the system to be charge recombined in the trajectories. Because we enforced a sudden electronic charge recombination without regard to the nuclear positions, the geometry may not have been in a physical state to form either the amide or the imidic acid tautomer, and instead was primed to form the unphysical Tyr-Gln adduct. In the experimental system, charge recombination and proton transfer are coupled in a manner that would avoid the formation of these unphysical adducts. In the main paper, we focused on the four trajectories that resulted in the Gln50 imidic acid tautomer for the light-adapted state.

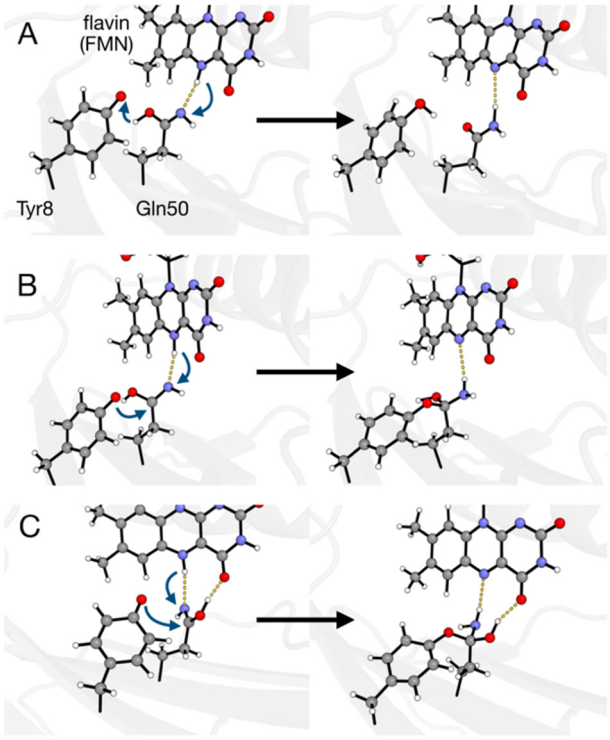

Fig. S2. Unproductive pathways observed in the simulation of reverse PCET in the Slr1694 BLUF photoreceptor. Of the nine trajectories propagated, four were productive in that they led to the imidic acid tautomer and are analyzed in the main text. Five were unproductive. Of the five unproductive trajectories, three followed the mechanism in A, which are the initial and final states (left and right, respectively) showing double proton transfer to reform the amide tautomer of Gln50. Panels B and C show the initial and final states for two additional unproductive pathways, where enforcing charge recombination led to the formation of an unphysical Tyr8-Gln50 adduct.

A.2 Protein preparation and equilibration for classical MD

The system preparation for the classical MD of the dark-adapted state (i.e., the Gln amide form) and the light-adapted state (i.e., the Gln imidic acid tautomer) closely followed the methodology used in our previous work. The Slr1694 BLUF photoreceptor with Gln50 in the amide form was obtained from the Protein Data Bank (PDB ID: 2HFN, 1.8 Å resolution).(11) Hydrogen atoms were added to these structures using the CHARMM HBUILD function assuming standard protonation states at pH 7. The structure for the Slr1694 BLUF photoreceptor with the

Gln50 imidic acid tautomer was obtained following 250 fs of ground state QM/MM dynamics for a trajectory that formed the imidic acid tautomer after the reverse PCET process, as described above, retaining the protein, FMN, and all solvent molecules within 3 Å of the protein structure. Given these structures for the amide and imidic acid Gln50 tautomer systems, we solvated each system in a periodically replicated cubic box of water molecules with side length 75.5 Å. Following solvation, Na^+ and Cl^- atoms were added to achieve charge neutrality and then to attain an approximately 0.150 M NaCl concentration. The CHARMM36 force field(12) was used for all amino acids and ions, in conjunction with the associated modified TIP3P water model.(13) The flavin force field parameters were obtained from a previous study on LOV domains,(14) as also used in previous MD studies of the AppA BLUF domain.(15) For the imidic acid tautomer, we parameterized a new force field, with the details given below. The particle mesh Ewald (PME)(16) method with a grid size of approximately 1 Å was used to compute electrostatic interactions, and the van der Waals interactions were treated with the SHIFT scheme and truncated at 14.5 Å. Bonds involving hydrogen were constrained with the SHAKE algorithm.(10) A 1 fs time step was used for all MD simulations.

For the two systems, equilibration was performed according to the following procedure with the CHARMM MD package.(8) For each system, the protein was fixed, and the solvent was minimized by 500 steps of steepest descent, followed by 10000 steps of adopted basis Newton-Raphson (ABNR), with a gradient tolerance of 0.01 kcal mol^{-1}. Next, with the protein still fixed, the solvent was heated from 100 K to 300 K over 20 ps, and then equilibrated at 300 K using velocity rescaling over the course of 250 ps. Then the solvent was equilibrated at 300 K for 250 ps using velocity rescaling followed by a 750 ps NVE ensemble trajectory. Subsequently, keeping the solvent fixed, the protein was minimized by 500 steps of steepest descent, followed by 10000

steps of ABNR, with a gradient tolerance of 0.01 kcal mol^{-1}. Restraining the protein heavy atoms to their optimized positions with a mass-weighted harmonic restraint of 1.0 kcal mol^{-1} $Å^{-2}$, the system was heated in the NVT ensemble from 100 K to 300 K over the course of 20 ps and then allowed to equilibrate at 300 K for a total of 250 ps. Subsequently, a harmonic restraint of 0.5 kcal mol^{-1} $Å^{-2}$ was used for an additional 250 ps of velocity rescaling equilibration at 300 K. Finally, all restraints were removed, and 500 ps of velocity rescaling equilibration at 300 K was performed.

Following this system preparation, each state was propagated for 20 ns with the NPT ensemble (300 K, 1 atm) using a Langevin thermostat with a collision frequency of 5 ps^{-1} and a Monte Carlo barostat to maintain constant pressure with the OpenMM MD package.(17) The box sizes stabilized with the sides of approximately length 74 Å. At the end of these 20 ns MD trajectories, each system was considered to be equilibrated.

A.3 QM/MM calculations of the flavin absorption spectrum and C4=O carbonyl stretch frequency

Following equilibration, each system was propagated for 5 ns with the NPT ensemble, and conformations were extracted every 10 ps to obtain a total of 500 conformations. For each conformation, the lowest ten electronic excited states were computed using electronically embedded time-dependent density functional theory (TDDFT) at the LRC-ωPBEh/6-31++G**/MM level of theory using the same QM region as described above. To avoid any potential unphysical electronic polarization due to solvent, each protein conformation was re-centered and aligned in its solvent box prior to computing the absorption spectrum, as done in previous work.(15, 18, 19) In order to obtain an ensemble-averaged electronic absorption spectrum

$S(\omega)$ as a function of energy ω for N individual spectra, each peak was dressed with a Gaussian function and summed according to the expression

$$S(\omega) = \frac{1}{N}\sum_{n,m} f_{nm} \cdot \exp[-4\ln(2)\,(\omega - \omega_{nm})^2/\gamma^2] \quad (1)$$

where n denotes the conformation and m denotes the particular excited state with corresponding energy ω_{nm} and oscillator strength f_{nm}. γ is an empirical broadening parameter that corresponds to the full-width at half-maximum of the associated Gaussian function. For all computed spectra given in the manuscript, γ corresponds to 10 nm.

To calculate the flavin C4=O carbonyl stretch frequency, we used the Fourier grid Hamiltonian (FGH) method,(20) where the one-dimensional Schrödinger equation was solved numerically for potential energy curves associated with the C4=O stretch for an ensemble of solvated protein conformations. To this end, we used 50 conformations obtained from the 5 ns trajectories for both the amide and imidic acid tautomer systems to compute the ensemble-averaged absorption spectra. Starting from a gas-phase optimized flavin isoalloxazine ring, we generated a potential energy curve corresponding to the C4=O stretch in normal mode coordinates, producing a total of 40 geometries, approximately sampling the CO distance between 0.9 and 1.8 Å. These flavin geometries were inserted into the electrostatic solvated protein environment by minimizing the RMSD with the existing flavin geometry. The electrostatically embedded single point energies at the LRC-ωPBEh/6-31++G**/MM level of theory were used to generate a potential energy curve that was interpolated via splining. Note that the flavin isoalloxazine ring is relatively rigid, and therefore inserting the flavin geometries into the protein environment corresponds to moving the carbon, oxygen, and neighboring atoms of the flavin along the relevant

mode to produce the potential energy curve associated with the C4=O stretch within the protein. The FGH method was used to solve the corresponding one-dimensional Schrödinger equation for each conformation using the normal mode mass obtained from the gas-phase frequency calculations, and the C4=O vibrational frequency was obtained as the energy difference between the lowest two eigenvalues corresponding to the vibrational energy levels. The shortest and longest C4=O carbonyl stretch distances studied exhibited electronic energies approximately 150 kcal/mol higher than the energy at the equilibrium distance, whereas the highest eigenvalue used to determine the frequency of the stretch mode was always between 7 and 8 kcal/mol. This large energy difference ensured that the FGH calculations were converged.

B. Additional computed flavin absorption spectra

B.1 Gas phase flavin absorption spectra using ensemble from main text with TDDFT

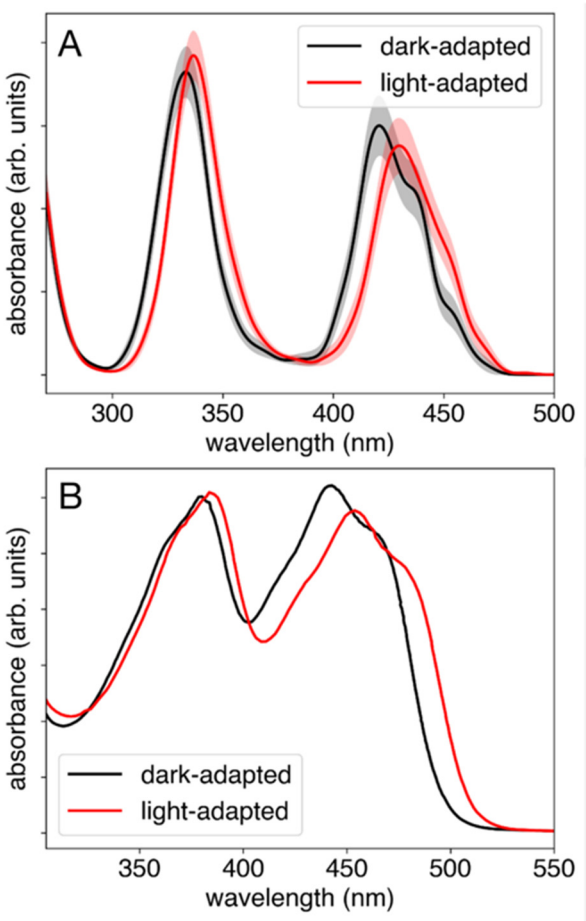

Fig. S3. Differences in the flavin absorption spectrum between the dark-adapted and light-adapted states of the Slr1694 BLUF photoreceptor. These calculations were performed at the TDDFT LRC-ωPBEh/6-31++G** level of theory and include only the QM region, excluding polarization from the classical MM environment. The computed ensemble spectra are given in (A) with the 95% confidence interval shaded, and the experimental absorption spectra (adapted from Ref. (21)) are given in (B). In both the computed and experimental spectra, the flavin S_1 peak at ~420 nm red shifts by ~10 nm in the light-adapted state compared to the dark-adapted state.

B.2 Flavin absorption spectra using ensemble from main text with TDA-TDDFT

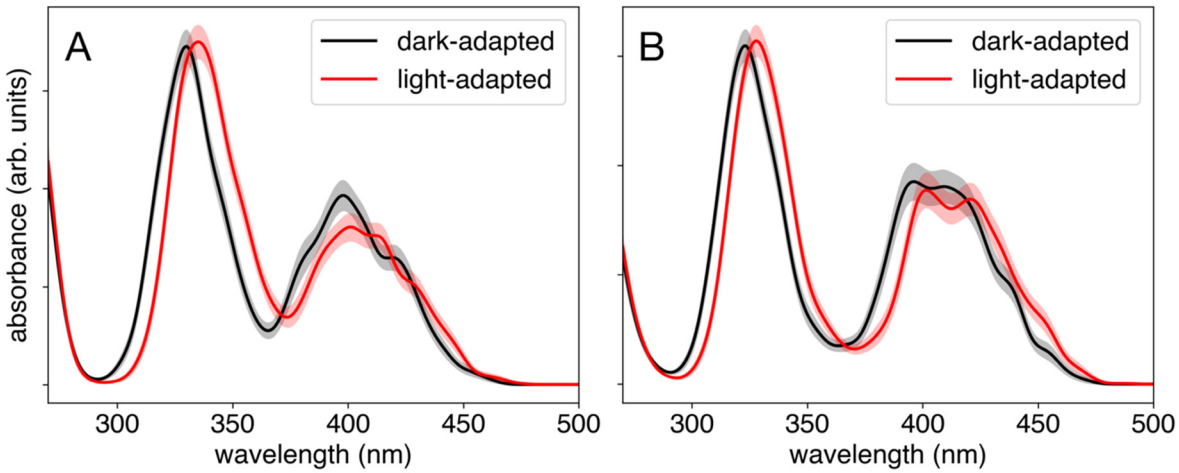

Fig. S4. Differences in the flavin absorption spectrum between the dark-adapted and light-adapted states of the Slr1694 BLUF photoreceptor. These calculations were performed at the TDA-TDDFT LRC-ωPBEh/6-31++G**/MM level of theory. The shaded region corresponds to the 95% confidence interval. The calculations given in (A) include the effects of the protein and solvent electrostatic environment, while the calculations in (B) include only the QM region, excluding polarization from the classical MM environment. In all computed spectra, the flavin S_1 peak at ~400 nm red shifts in the light-adapted state compared to the dark-adapted state, although neglecting polarization of the QM region due to the environment in (B) slightly reduces the computationally observed red shift.

B.3 Flavin absorption spectra using additional independent 5 ns ensemble with TDA-TDDFT

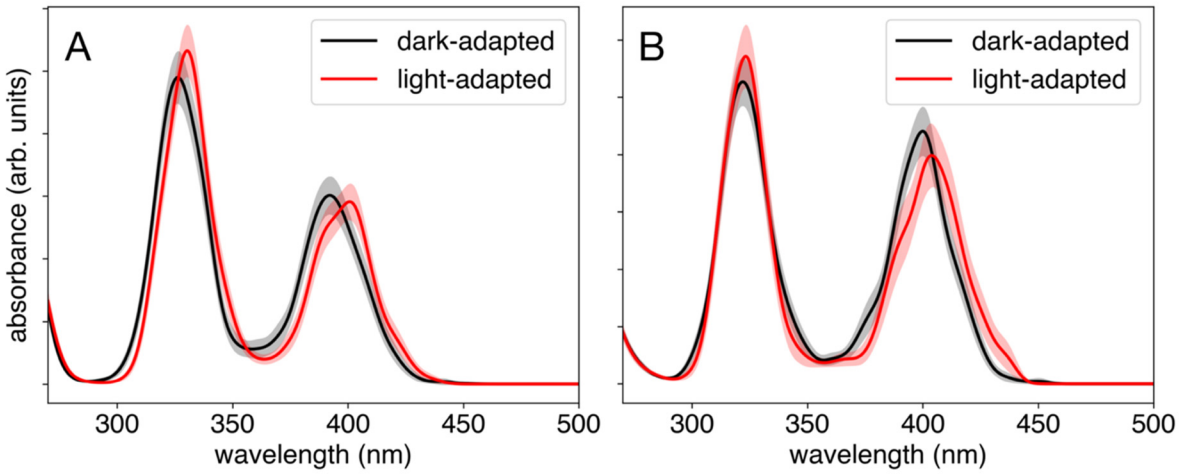

Fig. S5. Differences in the flavin absorption spectrum between the dark-adapted and light-adapted states of the Slr1694 BLUF photoreceptor for an independent data set composed of 500 conformations from a 5 ns NPT (300 K, 1 atm) trajectory. These calculations were performed at the TDA-TDDFT LRC-ωPBEh/6-31++G**/MM level of theory. The shaded region corresponds to the 95% confidence interval. The calculations given in (A) include the effects of the protein and solvent electrostatic environment, while the calculations in (B) include only the QM region, excluding polarization from the classical MM environment. In all computed spectra, the flavin S_1 peak at ~400 nm red shifts in the light-adapted state compared to the dark-adapted state.

C. Parameterization of the force field for the glutamine imidic acid tautomer

The force field Toolkit (ffTK)(22) plugin of the VMD program (version 1.9.3)(23) was used for the parameterization of charge, bond, and angle parameters for the Gln imidic acid tautomer. This protocol is consistent with the CHARMM force field(24) and CHARMM General Force Field (CGenFF).(25) Subsequently, the dihedral parameters were fitted manually. In the present parameterization, the quantum mechanical (QM) calculations were performed with the Gaussian09 program (version D.01),(26) while the molecular mechanical (MM) calculations were assisted by the CHARMM,(27) NAMD,(28) and AMBER(29) software packages. Specifically, the following procedures were performed to parameterize the sidechain of the Gln tautomer:

(1) Geometry of the model compound was optimized at the MP2/6-31G* level of theory, and a frequency analysis was performed to ensure that a minimum was found. The optimized geometry is shown in Fig. S5.

(2) During the charge fitting procedure, the partial charges of the CH_3 and CH_2 groups were fixed according to the CHARMM force field.(24) For the CH_3 group, the carbon has a charge of $-0.27e$, and each H has a charge of $+0.09e$, while for the CH_2 group, the carbon has a charge of $-0.18e$, and each H has a charge of $+0.09e$. The charges of the terminal C(NH)OH group were fitted based on the water-interaction profiles and the dipole moment of the model compound obtained by QM calculations. The water-interaction calculations were performed at the HF/6-31G* level of theory, while the dipole moment calculation was performed at the MP2/6-31G* level of theory. Specific adjustments were performed for the fitting, and these details can be found in the literature.(22)

(3) The missing bond and angle parameters were fitted based on the Hessian matrix calculated at the MP2/6-31G* level of theory and scaled by a factor of 0.889249. This factor is from the

square of the 0.943, which was found for the MP2/6-31G* level of theory to reproduce experimentally obtained vibrational frequencies.(30) Further details of this fitting can be found in the literature.(22)

(4) Subsequently, we parameterized the C-C-C-O, C-C-N-H, and C-C-O-H dihedral terms. The ffTK plugin employed a relaxed scan strategy for parameterizing the dihedral terms.(22) For the current system, however, the C-N-H angle becomes 180° when fixing the C-C-N-H dihedral angle as −90° or 90° along the relaxed scan at the MP2/6-31G* level of theory. This behavior was accompanied by a decrease in the C-N bond distance from 1.28 to 1.24 Å, most likely representing a switch from a double bond to a triple bond. The linearity of the C-N-H angle yields a large deviation from its equilibrium value in the force field, causing problems with the harmonic representation of this angle using a classical force field. Taking this issue into account, we used a rigid scan protocol to parameterize the missing dihedral terms. The missing dihedral parameters were fitted based on the potential energy surfaces obtained along rigid scans for the C-C-C-O, C-C-N-H, and C-C-O-H dihedral angles at the MP2/6-31G* level of theory. Each scan started from the optimized minimum obtained in Step 1 and was performed for 360° with increments of 15°. Finally, the missing dihedral terms were fitted based on these scans (see Fig. S6).

(5) To validate the quality of the force field developed for the Gln imidic acid tautomer, we compared the QM and MM optimized geometries (Fig. S5). Moreover, we compared the normal mode frequencies computed with QM to those computed with MM (Fig. S7). To be consistent with the previous steps, the QM calculated normal mode frequencies were obtained at the MP2/6-31G* level of theory and scaled by a factor of 0.943.

C.1 QM optimized geometry of the model compound

C 19.398973 -7.174757 -10.241844

H 19.130474 -6.195142 -9.842881

H 20.002766 -7.682868 -9.488075

C 18.152764 -7.983865 -10.570671

H 18.415426 -8.963144 -10.987747

H 17.549875 -7.486935 -11.339772

C 17.263590 -8.222546 -9.385285

N 17.542072 -7.781118 -8.218743

H 16.824624 -8.037697 -7.530667

H 20.004151 -7.034536 -11.141721

O 16.164707 -8.957080 -9.763791

H 15.601576 -9.100313 -8.979802

C.2 Atom types and partial charges for the Gln imidic acid tautomer

Atom	Atom type	Charges	Atom	Atom type	Charges
N	NH1	-0.470	HG2	HA2	0.090
HN	H	0.310	CD	CC1	0.745
CA	CT1	0.070	OE1	OH1	-0.618
HA	HB1	0.090	HE1	H	0.414
CB	CT2	-0.180	NE2	NH2	-0.869
HB1	HA2	0.090	HE22	H	0.328
HB2	HA2	0.090	C	C	0.510
CG	CT2	-0.180	O	O	-0.510
HG1	HA2	0.090			

C.3 Additional parameters for the CHARMM36 force field for the Gln imidic acid tautomer

ATOMS

MASS 84 CC1 12.01100

BONDS

!V(bond) = Kb(b - b0)**2

!Kb: kcal/mole/A**2

!b0: A

!atom type Kb b0

CT2 CC1 302.634 1.497 !

OH1 CC1 389.901 1.409 !

NH2 CC1 727.052 1.288 !

ANGLES

!V(angle) = Ktheta(Theta - Theta0)**2

!Ktheta: kcal/mole/rad**2

!Theta0: degrees

!atom types Ktheta Theta0

HA2 CT2 CC1 29.843 108.903 !

CT2 CT2 CC1 85.260 108.920 !

OH1 CC1 CT2 51.283 110.986 !

NH2 CC1 CT2 58.497 122.923 !

OH1 CC1 NH2 147.427 131.572 !

H OH1 CC1 71.608 114.925 !

H NH2 CC1 83.438 113.218 !

DIHEDRALS

!V(dihedral) = Kchi(1 + cos(n(chi) - delta))

!Kchi: kcal/mole

!n: multiplicity

!delta: degrees

!atom types Kchi n delta

CT1 CT2 CT2 CC1 0.1900 3 0.00 ! From X CT2 CT2 X

HA2 CT2 CT2 CC1 0.1900 3 0.00 ! From X CT2 CT2 X

CT2 CC1 OH1 H 1.7700 2 180.00 !

```
NH2  CC1  OH1  H       1.7700  2   180.00 !
H    NH2  CC1  CT2     1.4500  1     0.00 !
H    NH2  CC1  CT2     8.5900  2   180.00 !
H    NH2  CC1  OH1     8.5900  2   180.00 !
CT2  CT2  CC1  OH1     0.4000  1     0.00 !
CT2  CT2  CC1  OH1     0.3400  2   180.00 !
CT2  CT2  CC1  OH1     0.1500  3     0.00 !
HA2  CT2  CC1  OH1     0.1500  3     0.00 !
CT2  CT2  CC1  NH2     0.3400  2   180.00 !
HA2  CT2  CC1  NH2     0.0000  3     0.00 !

NONBONDED
!V(Lennard-Jones) = Eps,i,j[(Rmin,i,j/ri,j)**12 - 2(Rmin,i,j/ri,j)**6]
!epsilon: kcal/mole, Eps,i,j = sqrt(eps,i * eps,j)
!Rmin/2: A, Rmin,i,j = Rmin/2,i + Rmin/2,j
!atom  ignored    epsilon      Rmin/2
CC1    0.000000  -0.070000     2.000000 ! From CC
```

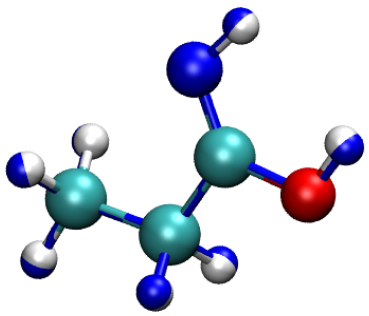

Fig. S5. Alignment of the QM optimized geometry (standard colors) and MM optimized geometry (blue). The root-mean-square deviation (RMSD) between the two structures is 0.035 Å.

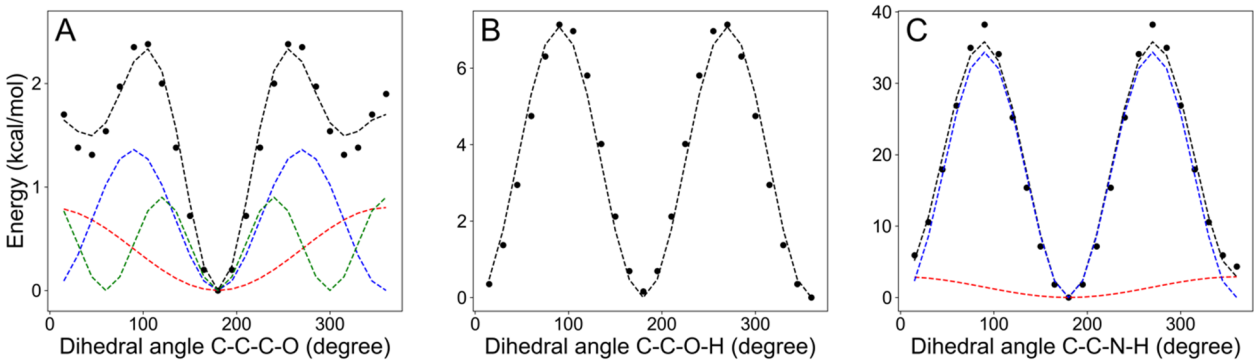

Fig. S6. The target potential energy surface (black dots) and fitted torsion term (black dash curves) for the dihedral angles (A) C-C-C-O, (B) C-C-O-H, and (C) C-C-N-H. The target potential energy surfaces were obtained as the differences between the potential energy surfaces of the QM and MM rigid scans along each dihedral angle, with the MM rigid scans setting these torsion terms to zero. For each of the C-C-C-O and C-C-N-H dihedral angles, multiple components were used, as depicted by dashed curves in green, red, and blue.

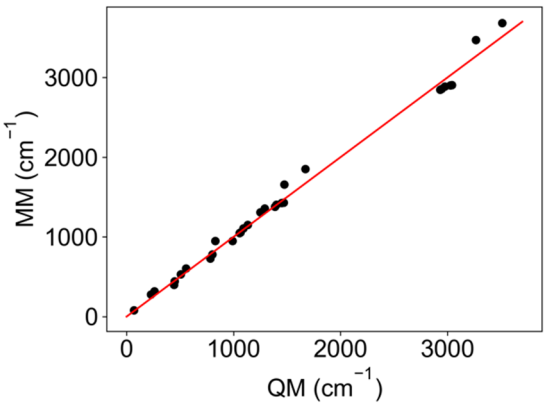

Fig. S7. Comparison of the normal mode frequencies for the Gln imidic acid tautomer calculated with the QM and MM methods, where the perfect match is depicted by the red line. The QM calculated frequencies were obtained at the MP2/6-31G* level of theory and scaled by a factor of 0.943.

References

1. J. J. Goings, S. Hammes-Schiffer, Early photocycle of Slr1694 blue-light using flavin photoreceptor unraveled through adiabatic excited-state quantum mechanical/molecular mechanical dynamics. *J. Amer. Chem. Soc.* **141**, 20470-20479 (2019).
2. W. J. Hehre, R. Ditchfield, J. A. Pople, Self-consistent molecular orbital methods. XII. Further extensions of Gaussian-type basis sets for use in molecular orbital studies of organic molecules. *J. Chem. Phys.* **56**, 2257-2261 (1972).
3. P. C. Hariharan, J. A. Pople, The influence of polarization functions on molecular orbital hydrogenation energies. *Theor. Chim. Acta* **28**, 213-222 (1973).
4. M. A. Rohrdanz, K. M. Martins, J. M. Herbert, A long-range-corrected density functional that performs well for both ground-state properties and time-dependent density functional theory excitation energies, including charge-transfer excited states. *J. Chem. Phys.* **130**, 054112 (2009).
5. X. Zhang, J. M. Herbert, Analytic derivative couplings for spin-flip configuration interaction singles and spin-flip time-dependent density functional theory. *J. Chem. Phys.* **141**, 064104 (2014).
6. Y. Shao, M. Head-Gordon, A. I. Krylov, The spin–flip approach within time-dependent density functional theory: Theory and applications to diradicals. *J. Chem. Phys.* **118**, 4807-4818 (2003).
7. H. L. Woodcock, 3rd *et al.*, Interfacing Q-Chem and CHARMM to perform QM/MM reaction path calculations. *J. Comput. Chem.* **28**, 1485-1502 (2007).
8. B. R. Brooks *et al.*, CHARMM: the biomolecular simulation program. *J. Comput. Chem.* **30**, 1545-1614 (2009).
9. Y. Shao *et al.*, Advances in molecular quantum chemistry contained in the Q-Chem 4 program package. *Mol. Phys.* **113**, 184-215 (2015).
10. J.-P. Ryckaert, G. Ciccotti, H. J. C. Berendsen, Numerical integration of the cartesian equations of motion of a system with constraints: molecular dynamics of n-alkanes. *J. Comput. Phys.* **23**, 327-341 (1977).
11. H. Yuan *et al.*, Crystal structures of the Synechocystis photoreceptor Slr1694 reveal distinct structural states related to signaling. *Biochemistry* **45**, 12687-12694 (2006).
12. R. B. Best *et al.*, Optimization of the additive CHARMM all-atom protein force field targeting improved sampling of the backbone ϕ, ψ and side-chain $\chi1$ and $\chi2$ dihedral angles. *J. Chem. Theory Comput.* **8**, 3257-3273 (2012).
13. W. L. Jorgensen, J. Chandrasekhar, J. D. Madura, R. W. Impey, M. L. Klein, Comparison of simple potential functions for simulating liquid water. *J. Chem. Phys.* **79**, 926-935 (1983).
14. P. L. Freddolino, K. H. Gardner, K. Schulten, Signaling mechanisms of LOV domains: new insights from molecular dynamics studies. *Photochem. Photobiol. Sci.* **12**, 1158-1170 (2013).
15. P. Goyal, S. Hammes-Schiffer, Role of active site conformational changes in photocycle activation of the AppA BLUF photoreceptor. *Proc. Natl. Acad. Sci. U. S. A.* **114**, 1480-1485 (2017).
16. T. Darden, D. York, L. Pedersen, Particle mesh Ewald: An N·log(N) method for Ewald sums in large systems. *J. Chem. Phys.* **98**, 10089-10092 (1993).

17. P. Eastman *et al.*, OpenMM 7: Rapid development of high performance algorithms for molecular dynamics. *PLOS Comput. Biol.* **13**, e1005659 (2017).
18. E. R. Sayfutyarova, J. J. Goings, S. Hammes-Schiffer, Electron-coupled double proton transfer in the Slr1694 BLUF photoreceptor: A multireference electronic structure study. *J. Phys. Chem. B* **123**, 439-447 (2018).
19. J. J. Goings, C. R. Reinhardt, S. Hammes-Schiffer, Propensity for proton relay and electrostatic impact of protein reorganization in Slr1694 BLUF photoreceptor. *J. Am. Chem. Soc.* **140**, 15241-15251 (2018).
20. D. J. Tannor, *Introduction to quantum mechanics: a time-dependent perspective* (University Science Books, 2007).
21. S. Masuda, K. Hasegawa, A. Ishii, T.-a. Ono, Light-induced structural changes in a putative blue-light receptor with a novel FAD binding fold sensor of blue-light using FAD (BLUF); Slr1694 of Synechocystis sp. PCC6803. *Biochemistry* **43**, 5304-5313 (2004).
22. C. G. Mayne, J. Saam, K. Schulten, E. Tajkhorshid, J. C. Gumbart, Rapid parameterization of small molecules using the force field toolkit. *J. Comput. Chem.* **34**, 2757-2770 (2013).
23. W. Humphrey, A. Dalke, K. Schulten, VMD: visual molecular dynamics. *J. Mol. Graph.* **14**, 33-38 (1996).
24. A. D. MacKerell *et al.*, All-atom empirical potential for molecular modeling and dynamics studies of proteins. *J. Phys. Chem. B* **102**, 3586-3616 (1998).
25. K. Vanommeslaeghe *et al.*, CHARMM general force field: A force field for drug-like molecules compatible with the CHARMM all-atom additive biological force fields. *J. Comput. Chem.* **31**, 671-690 (2010).
26. M. J. Frisch *et al.* (2013) Gaussian 09, Revision D. 01. (Gaussian Inc., Wallingford, CT).
27. B. R. Brooks *et al.*, CHARMM: the biomolecular simulation program. *J. Comput. Chem.* **30**, 1545-1614 (2009).
28. J. C. Phillips *et al.*, Scalable molecular dynamics with NAMD. *J. Comput. Chem.* **26**, 1781-1802 (2005).
29. D. A. Case *et al.*, The Amber biomolecular simulation programs. *J. Comput. Chem.* **26**, 1668-1688 (2005).
30. A. P. Scott, L. Radom, Harmonic vibrational frequencies: an evaluation of Hartree− Fock, Møller− Plesset, quadratic configuration interaction, density functional theory, and semiempirical scale factors. *J. Phys. Chem.* **100**, 16502-16513 (1996).